

Novel method for the identification of the maximum solid loading suitable for optimal extrusion of ceramic pastes

Andrea AZZOLINI*, Vincenzo M. SGLAVO, John A. DOWNS

Department of Industrial Engineering, Università di Trento, Via Mesiano 77, 38123, Trento, Italy

Received: July 11, 2013; Revised: October 30, 2013; Accepted: November 12, 2013

©The Author(s) 2014. This article is published with open access at Springerlink.com

Abstract: Gadolinia-doped ceria ceramic pastes were formulated with different solid loadings and extruded using lab-scale equipment. The force to maintain a constant ram speed of 10 mm/min was recorded. The radial shrinkage after drying was proportional to the solid loading and this allowed the determination of the maximum solid loading by an extrapolation procedure. In order to obtain the apparent viscosity of the pastes, a novel approach based on the analysis of the slope of the extrusion pressure plot versus distance covered by the ram, was formulated for the direct determination of the shear stress upon extrusion. The agreement of the determined maximum solid loading with values calculated by two existing models confirmed that the proposed approach was an alternative and reliable method to identify the upper limit of the solid loading range for the formulation of extrudable ceramic pastes.

Keywords: ceramic extrusion; maximum solid loading; drying shrinkage; rheology

1 Introduction

Extrusion is a fast and reliable forming technique for the fabrication of long objects with constant cross section. It allows for high production rates while maintaining dimensional accuracy and an optimal surface finish [1–4]. Though extrusion has been mostly developed for polymeric and metallic materials, it has also found numerous applications for technical ceramic products. It is currently used in the ceramic industry for the manufacturing of different shapes, ranging from the very simple, such as clay bricks, to very complicated articles, such as ceramic honeycomb

matrices used in a car exhaust system to control and limit pollutant emissions. Nevertheless, the process of ceramic extrusion still lacks of a systematic knowledge and the literature regarding this field is relatively scarce.

An extrusion paste is generally composed of a solid phase and a liquid phase. For the extrusion of ceramic objects, the solid phase is composed by ceramic powder with particle sizes ranging typically between 0.1 μm and 100 μm . The liquid phase has the role of surrounding and separating particles from each other and facilitating their mutual sliding. Also, the capillary force generated by liquid bridges between the particles in a deflocculated system, is believed to be the main component of the cohesive force that keeps the particles together in a coherent plastic mass [5]. Water alone is not sufficient to formulate an extrudable paste if the solid phase is not clay. In fact, the liquid phase

* Corresponding author.
E-mail: andrea.azzolini@ing.unitn.it

must possess non-Newtonian behavior of visco-plastic type, that is, being characterized by the existence of a threshold stress (called yield stress or apparent yield stress), which must be exceeded for the fluid to deform and flow. This behavior can be achieved by adding thermoplastic polymers or other organics like, for example, cellulose in water [6–9]. The organic agents allow for close control of the paste viscosity and act as a binder in the green extrudate once water has been removed by drying, imparting the necessary resistance for handling and avoiding the breakage of the green body.

The ratio of the volume of the solid phase to the total volume of the paste is defined as the solid loading, and is the main characteristic that influences the flow behavior and the extrudability of the paste. From a quantitative point of view, it is important to define the solid loading corresponding to the exact liquid volume required to fill the interparticle volume in a loose-packed configuration, which is typically called the critical volume fraction or maximum solid loading (ϕ_m). Only when the solid loading is lower than ϕ_m , the paste can be extruded because the liquid layer surrounding the solid particles is thick enough to allow their sliding. However, if the solid loading is too low, the paste will behave like a viscous suspension and not be able to retain the extruded shape. Conversely, for solid loadings increasing and tending to ϕ_m , the liquid phase present is not adequate to allow for easy particle sliding. This is responsible for large frictional force resulting in a rapid increase of the extrusion pressure that can quickly exceed equipment limit. If ϕ_m is eventually attained or exceeded, the paste loses its ability to flow and the viscosity tends to infinity [10]. If the solid loading is optimized, the paste is soft enough to be formed with moderate extrusion pressure but also sufficiently strong to minimize deformations of the extruded green shape. An accurate experimental determination of ϕ_m is important for a successful formulation of the ceramic paste and several methods have been proposed in the literature [11–14].

After extrusion, most of the liquid phase is removed during successive drying; therefore, the solid loading has a considerable influence not only on the flow properties of the paste but also on the drying shrinkage and, consequently, on the green and sintered densities of the extrudate [15].

The present work was developed as part of a larger

project for the fabrication of solid oxide fuel cell (SOFC) anodes and electrolytes. With the aim of obtaining a dense sintered structure, as in the case of electrolytic layers in SOFC, it was necessary to look for a value of the solid loading as high as possible, to reach high green and sintered density, compatibly with maintaining good flow properties and moderate extrusion pressures. Therefore, the influence of solid loading on the shrinkage upon drying and on the green and sintered density of extruded gadolinia-doped ceria was investigated, and a novel procedure for the determination of the maximum solid loading was proposed.

2 Materials and methods

The preparation of an extrusion paste typically follows several successive stages, which aim to the optimal mixing of the components and the production of a homogeneous distribution of the two phases (e.g., liquid and solid) [16]. In the present work, the ceramic powder used was commercially available gadolinia-doped (10 mol%) ceria (CGO10, $D_{50}=0.27\ \mu\text{m}$, $\text{BET}=9.10\ \text{m}^2/\text{g}$, Treibacher Industries, Austria). Hydroxypropyl methyl-cellulose (HPMC, Sigma Aldrich, $\text{MW}\approx 22\ \text{kDa}$) was used as binder and thickening agent as 2 wt% based off of the liquid phase for each solid loading value studied. The solid components were dry-mixed together in a planetary mixer for 3 h. The mixed powder was then slowly added to bi-distilled water to reach the requested solid loading, which was evaluated as

$$\phi = \frac{m / \rho_{\text{th}}}{m / \rho_{\text{th}} + V} \quad (1)$$

where m is the mass of the powder; ρ_{th} is its theoretical density; and V is the volume of the liquid phase. ϕ provisionally ranges between 40 vol% and 50 vol%.

The latter step (i.e., wet mixing) was carried on using a kneading hook mounted on a vertical shaft mixer for about 15 min until all water was completely absorbed and the paste was homogeneous. The paste was then extruded through a flat die with several small holes of 4 mm in diameter. This high shear-mixing step contributed to further homogenize the paste and break any remaining agglomerates. The paste was then placed in a sealed plastic bag and stored overnight in humidified vessel at room temperature to avoid any

change in water content.

The extrusion procedure was performed by an in-house built aluminum ram extruder (Fig. 1). It was constituted of a barrel with an internal diameter of 23 mm and a loading capacity of 60 cm³ inside of which a ram slides. An O-ring placed on the final part of the ram ensured a sufficient seal with the barrel wall. The internal surface of the cylinder was carefully polished to mirror finishing with diamond paste to reduce the friction with the piston. The die used in this work was 23.13 mm in length and 5.1 mm in diameter. The upper part of the piston was fitted to a 100-kN load cell on a universal mechanical testing machine (MTS, mod. 810) that allowed the recording of the load required to keep the ram speed constant at 10 mm/min during the whole process. The extruded samples were collected within the grooves of a sample holder specifically realized by highly porous alumina to avoid differential water evaporation and warping upon drying.

The green samples were dried slowly for the first hour in a humid environment (relative humidity of ca. 86%) and then overnight in presence of silica salts at room temperature. The remaining drying was carried out in an oven at 110 °C for 4 h. The bulk densities of the green samples were evaluated subtracting the net weight of the binder.

The dried samples were heated at 2 °C/min up to a de-binding temperature of 500 °C, maintained for 1 h,

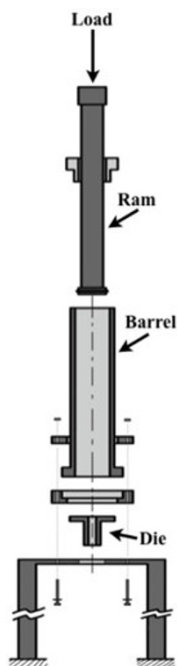


Fig. 1 Lab-scale ram extruder used in this work.

and then at 5 °C/min up to the sintering temperature of 1550 °C that was kept for 2 h. The bulk densities were measured by the Archimedes method. The densification behavior of the green samples was measured by dilatometry (Linseis L75) from room temperature to 1550 °C with a constant heating rate of 5 °C/min. The dilatometric shrinkage data were then converted into densification curves [17]. Microstructure examination was performed by scanning electron microscopy (SEM, Jeol, JSM5500) on manually produced fracture surfaces.

3 Results and discussion

3.1 Influence of solid loading on the extrusion pressure

During extrusion, the force on the load cell was monitored as a function of the distance travelled by the ram. The force can be decomposed into a shaping component, associated to the deformation of the plastic mass through the die, and a friction component, related to the slip of the paste on the barrel and die internal walls during flow. Supposing that the rheological characteristics of the paste do not change during the whole extrusion process, the shaping component, which is related to the plastic yield stress of the paste, and the die friction component remain constant, while the barrel friction component decreases as the ram advances and the wetted barrel surface decreases. The typical plot of an extrusion process, accordingly, shows an initial zone of slow pressure increase due to the flattening of the paste in the barrel, followed by an abrupt increase due to the die filling. The pressure plot flattens as soon as the paste starts to be extruded and, depending on the value of friction between paste and barrel, decreases as the less of the barrel surface wetted by the paste, eventually reaching a minimum. The Benbow–Bridgewater model well indicates the dependence of the minimum value of the extrusion pressure from the geometrical characteristics of the extruder and some rheological parameters of the paste as shown by Eq. (2) [16]:

$$P = P_e + P_f = 2(\sigma_0 + \alpha V^n) \ln\left(\frac{D_0}{D}\right) + 4(\tau_0 + \beta V^m) \left(\frac{L}{D}\right) \quad (2)$$

where α is a velocity-dependent factor for the convergent flow; β is the velocity-dependent factor

for parallel flow; m and n are the exponents of the extrudate velocity; σ_0 is the paste bulk yield value; τ_0 is the paste shear yield stress; D_0 and D are the diameters of the barrel and the die, respectively; L is the die-land length; and V is the extrudate velocity. In this equation, the pressure is obtained as the sum of two contributions: one from the die-entry (P_e) and one from the die-land (P_1).

The subsequent pressure increase is recorded when the ram is about to enter the static zone near the die. The paste located in the bottom portion of the barrel around the die, also called dead zone, can hardly flow due to sharp corners. This usually causes a steep rise in pressure toward the end of the process. Figure 2 shows the plots corresponding to the extrusion of two pastes with solid loading of 44 vol%, one of them having been subjected to the high shear-mixing procedure before extrusion.

The process steps described above are clearly shown. The plot corresponding to the highly shear-mixed paste (paste A) exhibits a reduction of the extrusion pressure of about 30%. Moreover, the surface finish was considerably better in this case, indicating that the high shear mixing contributes to further homogenize the paste and break down any agglomerate created during the wet mixing phase.

When the pressure gradients during the extrusion are large, typically because of high plastic yield stress, liquid phase migration phenomena can occur and the rheological characteristic of the paste can locally change with time [18,19]. If this is the case, the paste inside the barrel is drier than the extruded one. This causes a further consolidation of the paste and the quick rise of both the shaping and the friction components of the extrusion force [18]. The liquid

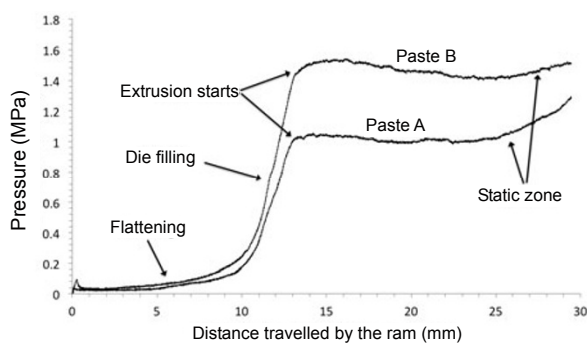


Fig. 2 Extrusion pressure as a function of the distance travelled by the ram for two pastes with 44 vol% solid loading. Paste A was subjected to high shear mixing before extrusion.

phase migration and the corresponding paste consolidation result to be also dependent on the extrusion velocity and modify substantially the flow typology [18,19]. The effect of the liquid migration can be observed in Fig. 3, which shows the extrusion pressure for pastes prepared with solid loading ranging between 40 vol% and 50 vol%.

When the solid loading is increased, the liquid volume available for the mutual flow of the particles is lower and this leads to a higher plastic yield stress and a higher value of pressure required to activate the extrusion process. For 40 vol% solid loading, the pressure is approximately constant and thus, the friction with the barrel can be considered negligible. Therefore, the only contribution for this paste comes from the shaping and the die friction forces that are constant, assuming that no liquid migration is clearly observed. For solid loadings of 42–46 vol%, a slight decrease in pressure is shown in the stable operation step until the pressure rises for effect of the static zone. The 48 vol% solid loading paste exhibits a noisier signal as a result of considerable friction with the extruder walls. The liquid phase is too scarce and does not allow an efficient flow of the paste. The higher pressure required for the extrusion causes the migration of the liquid phase as indicated by the early and steep rise of the final part of the signal. This dewatering effect is even more significant for the paste with 50 vol% solid loading. It does not show any plateau of stable operation but a continual increase of pressure up to the extruder pressure limit set at 8.5 MPa. Considering the extrusion pressure as the minimum value assumed by the pressure during the stable operation, its dependence on solid loading is represented in Fig. 4. For the 50 vol% paste, seeing the

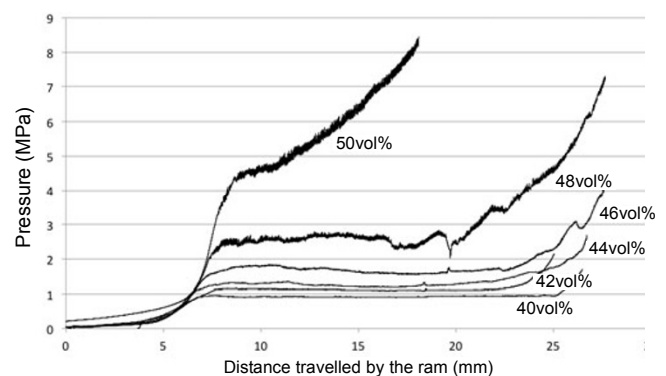


Fig. 3 Extrusion pressure as a function of the distance travelled by the ram for pastes with various solid loadings.

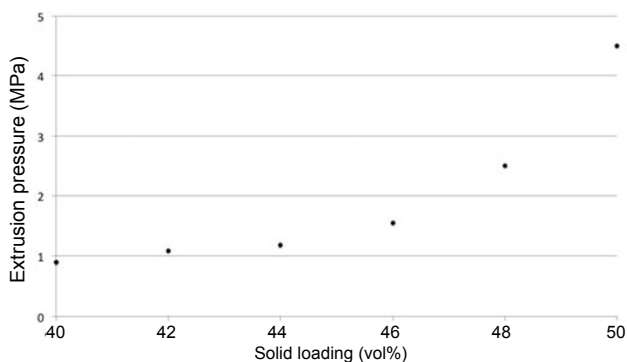


Fig. 4 Evolution of the extrusion pressure with solid loading.

absence of a minimum, the extrusion pressure can be considered equal to the minimum value assumed by the pressure from the moment when the paste is extruded.

3.2 Drying shrinkage and green density

During drying, the liquid phase is removed from the extrudate and the powder particles pack together. The mechanism is very similar to that proposed for the initial stage of liquid-phase sintering [14] and leads to an overall shrinkage of the samples and an increase of the green density [20]. Generally, drying proceeds through two main steps. During the first one, liquid flows through the pores from the interior to the sample surface and evaporates there. The water loss is linear in time with rate depending on the sample geometry, the vapor pressure and the temperature. As the meniscus radius decreases, the pores start to shrink and the density of the green body increases correspondingly until the powder particles touch each other. During the following drying step, the drying rate slows down: the liquid–vapor meniscus starts to retreat inside the pores

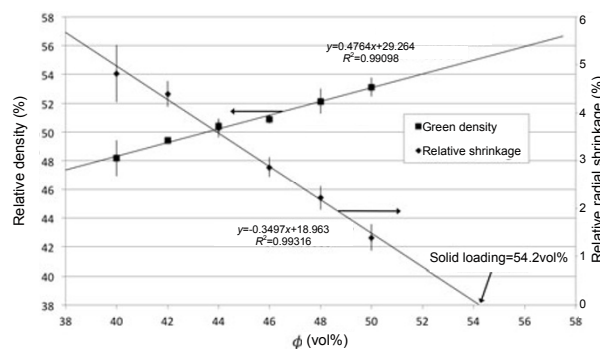


Fig. 5 Relative bulk density of the green extrudate and radial shrinkage for dried sample as a function of the solid loading; the standard deviation is also shown. Continuous lines correspond to linear fitting of the experimental average data (fitting equations and correlation coefficient are also shown). The graphical construction used to determine the maximum solid loading is also shown.

and the transport of liquid to the surface is the rate-limiting mechanism. The liquid that cannot reach the surface has to evaporate within the pores, further decreasing the drying rate [21,22]. Higher liquid content corresponds to larger shrinkage. In the analyzed range, the radial shrinkage during drying depends linearly on the solid loading as shown in Fig. 5.

The average relative bulk density of the dried extrudate, represented in Fig. 5, also follows a linear relationship with respect to the solid loading [15]. It is evident that a larger shrinkage leads to a larger difference between the dried green density and the initial solid loading of the paste. The samples formulated with 40 vol% solid loading become ~8% denser upon drying, while samples with 50 vol% solid loading increase their density of ~3%. Although the shrinkage during drying does not bring every sample to

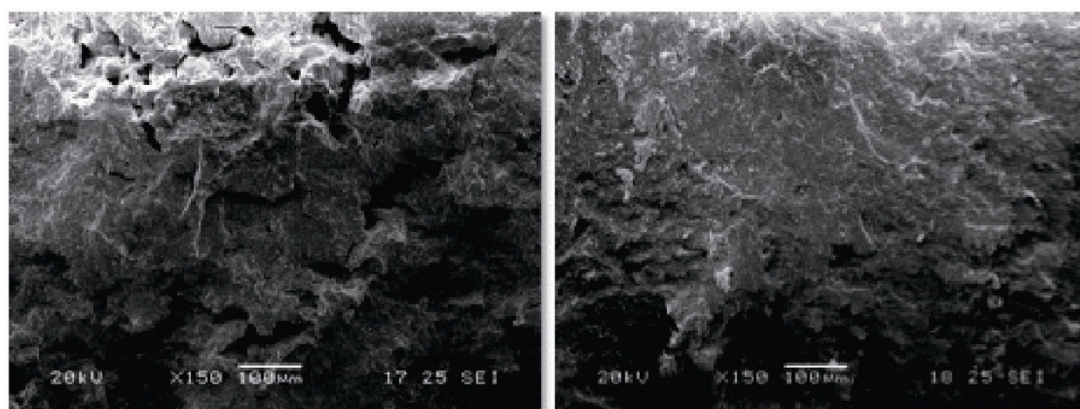


Fig. 6 SEM micrographs of fracture surface for green samples with 40 vol% (left) and 50 vol% (right) solid loadings.

the achievement of the same final bulk density, the larger is the shrinkage, the smaller is the density achieved by the dried green sample. Also, the packing resulting from large shrinkage is lower than the one relative to small shrinkage. In other words, the drying mechanism appears to have worst efficiency for lower solid loadings, resulting in a lower green density. This is confirmed also by microstructural SEM analyses reported in Fig. 6 where samples at 40 vol% and 50 vol% are compared, indicating that lower packing efficiency corresponds to the presence of unfilled macroporosity during drying.

It can be interesting to observe that the extrapolation of the shrinkage linear trend intersects the x -axis relative to no shrinkage effect (Fig. 5) at a value of 54.2 vol% of solid loading. Such value can be associated to the solid loading of a paste that is not subjected to density increase during drying and therefore to the maximum solid loading, ϕ_m , suitable for the specific powder.

3.3 Sintered density and densification rates

The densification curves were recorded for samples formulated with different solid loadings and they show very similar trend in Fig. 7. The final density reached after the heating cycle depends primarily on the bulk density of the dried green body, as already observed in literature for samples obtained by other production techniques [23–25]. The densification kinetic is also a function of the green density: the maximum densification rate is slightly faster for higher solid loadings although the overall difference is negligible considering the values ranged between 0.82%/min and 0.87%/min (Fig. 8). Even for what concerns the temperature of maximum densification, it appears to be the same for every analyzed sample, around 1380 °C.

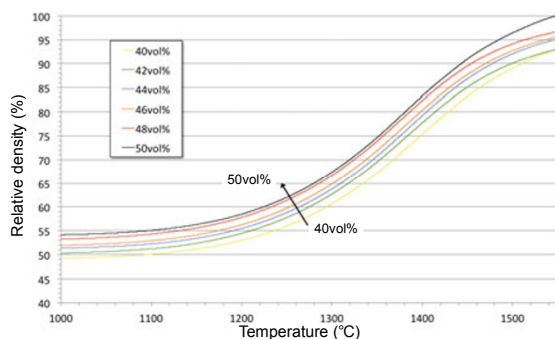


Fig. 7 Densification of green extrudates upon heating for solid loadings ranging between 40 vol% and 50 vol%.

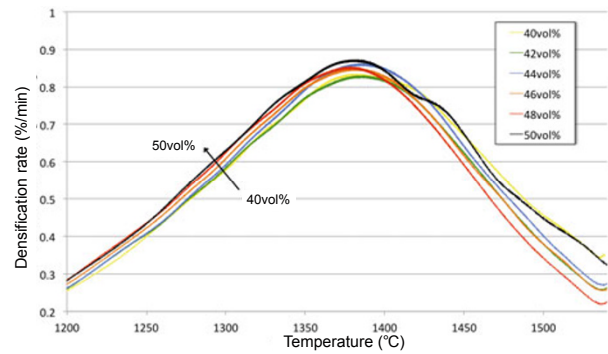


Fig. 8 Densification rate of green extrudates upon heating for solid loadings ranging between 40 vol% and 50 vol%.

The relative bulk density obtained after sintering at 1550 °C for 2 h and calculated as $\rho_r = \rho_b / \rho_{th}$ (where ρ_b is the measured bulk density and ρ_{th} is the real density of CGO10 = 7.22 g/cm³) is reported in Table 1. The samples with solid loading higher than 42 vol% achieve relative density higher than 97% and can be considered as fully dense. These observations confirm the influence of the presence of residual porosity in the green extrudate (Fig. 6) on the final microstructure.

From the precedent observations, it is possible to obtain a criteria for the experimental determination of the correct solid loading for the extrusion of ceramic bodies. If an high solid loading paste allows to obtain samples experiencing small shrinkages and with less possibilities of damaging during drying, its extrusion leads to the onset of large extrusion pressures that are often associated with de-watering effects. Contrarily, a paste with low solid loading minimizes the extrusion pressure, avoiding de-watering and damaging of the extruder, but it is also associated to large drying shrinkages and lower green/sintered densities.

3.4 Prediction of viscosity of extrusion pastes

The maximum solid loading, ϕ_m , previously obtained from the linear extrapolation of the drying shrinkage is here compared with the values that can be calculated from the analysis of the paste viscosity on the basis of

Table 1 Relative density after sintering as a function of the initial solid loading

ϕ (vol%)	ρ_r (%)	ϕ (vol%)	ρ_r (%)
40	94.6	46	98.5
42	96.3	48	99.3
44	97.5	50	99.1

previous reported studies. There are numerous semi-empirical models that allow to predict the viscosity of highly concentrated ceramic suspensions [1]. In the present work, two of them are considered: the most widely used Krieger–Dougherty equation [26]:

$$\eta = \eta_0 \left[1 - \left(\frac{\phi}{\phi_m} \right) \right]^{-[\eta]\phi_m} \quad (3)$$

and the Reddy equation [27], based on the rule of mixtures:

$$\eta = \eta_0 \left(\frac{\phi_m}{\phi_m - \phi} \right) \quad (4)$$

where η_0 is the viscosity of the pure liquid medium; $[\eta]$ is an empirically derived hydrodynamic crowding factor defined as intrinsic viscosity.

The parameters η_0 , $[\eta]$ and ϕ_m are typically obtained by fitting procedure of the experimental data. The apparent viscosity of ceramic pastes, considered to be non-Newtonian fluids, is given by the ratio between the true shear stress and the apparent shear strain at the die wall:

$$\eta_a = \frac{\tau_w}{\dot{\gamma}_a} \quad (5)$$

The shear stress for a circular die depends on the geometry and the pressure gradient along it. It can be calculated considering the sum of the forces acting on a cylindrical element subjected to steady laminar flow [28]:

$$\tau_w = \frac{R}{2} \left(\frac{\partial P}{\partial z} \right) = \frac{R}{2} \frac{\Delta P}{L} \quad (6)$$

where ΔP is the pressure variation along the extremes of the die of length L and radius R ; and the right term is obtained by integrating the pressure gradient, considered linear, along the die. Nonetheless, as pointed out before, the pressure recorded by the load cell above the piston includes also contributions due to the friction with the barrel and the shaping force needed to modify the section of the paste from the barrel to the die. To isolate the contribution to the pressure gradient due to the flow along the die only, the Bagley correction is usually applied [29]. It allows to estimate the pressure drop at the die entrance and exit by linear extrapolation of the steady state pressure readings for dies of different lengths. The pressure drop extrapolated for die length equal to zero is then subtracted to any other pressure readings to obtain the value of the true shear stress. Nevertheless, in addition

to the requirement of several measurements, this correction is not always immediate since the obtained values can hardly be fitted linearly [30]. A further problem concerns the identification of the exact value of the extrusion pressure. As a matter of fact, often the pressure trend does not allow to distinguish univocally the steady state plateau, especially in the case of very tough pastes and liquid migration (Fig. 3).

Therefore, in the case of the measurements reported above, a more reliable reading of the pressure gradient along the die can be obtained from the analysis of the first stage of the extrusion plot, before the maximum pressure corresponding to the paste coming out from the die is reached. This phase is reported in Fig. 9 for extrusions of 40 vol% and 50 vol% solid loading pastes. As the plot clearly shows, the initial stage of extrusion is composed by three steps corresponding to three specific physical processes: a first phase of slow increase due to the flattening of the paste, a more steep increase due to the transfer of the paste to the die land and, eventually, a steady rise corresponding to the flow of the paste within the die.

In order to obtain the pressure gradient required in Eq. (6), it is sufficient to identify the slope of the line fitting the third phase and convert it into the die coordinates. Considering the ceramic paste as incompressible, the ram and the extrudate velocities are connected by the equation for volume conservation:

$$v_{extr} = \frac{A_0}{A} v_{ram} \quad (7)$$

where A_0 and A are the barrel and the die sections,

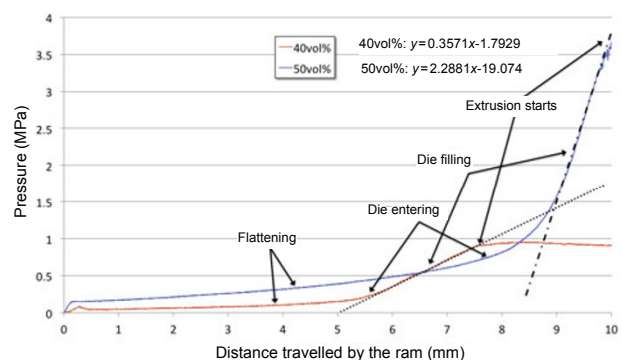


Fig. 9 Pressure recorded by the load cell during the initiation of extrusion process as a function of the movement of the ram for 40 vol% and 50 vol% solid loading pastes. In both cases, the steady rise corresponding to the flow within the die is well approximated by the reported linear equation.

respectively. Indicating with the ram displacement z_{ram} and the paste displacement inside the die z_{extr} , the pressure gradient becomes

$$\frac{\partial P}{\partial z_{extr}} = \frac{\partial P}{\partial z_{ram}} \frac{\dot{z}_{ram}}{\dot{z}_{extr}} = \frac{\partial P}{\partial z_{ram}} \frac{v_{ram}}{v_{extr}} = \frac{\partial P}{\partial z_{ram}} \frac{A}{A_0} \quad (8)$$

That, inserted in Eq. (6), allows the evaluation of the true die wall shear stress. The values obtained with this approach are reported in Fig. 10 for variable solid loadings.

The apparent shear rate can be evaluated as [28]:

$$\dot{\gamma}_a = \left(\frac{4Q}{\pi R^3} \right) \quad (9)$$

where Q is the flow rate through the capillary of radius R . The apparent viscosity of the pastes is given by Eq. (5) and well agrees with viscosities of extrusion pastes obtained by similar capillary rheometry measurements [27,28,30,31]. The apparent viscosity for different solid loadings is used for the determination of best fit parameters for Eqs. (3) and (4) linearized as follows:

Krieger–Dougherty:

$$\ln \eta = -[\eta] \phi_m \ln \left(1 - \frac{\phi}{\phi_m} \right) + \ln \eta_0 \quad (10)$$

Reddy:
$$\eta \phi = \eta \phi_m - \eta_0 \phi_m \quad (11)$$

The parameters ϕ_m , η_0 and $[\eta]$ are obtained by the linear fit of Eqs. (10) and (11) as shown in Fig. 11 and are reported in Table 2. A detailed description about the non-linear optimization of the parameters for the Krieger–Dougherty and other models, can be found elsewhere in literature.

As shown in Fig. 12, Eqs. (3) and (4) match very well the apparent viscosity experimental values

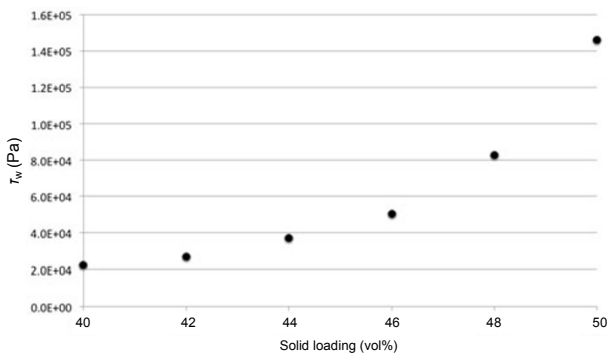


Fig. 10 True die wall shear stress for variable solid loading.

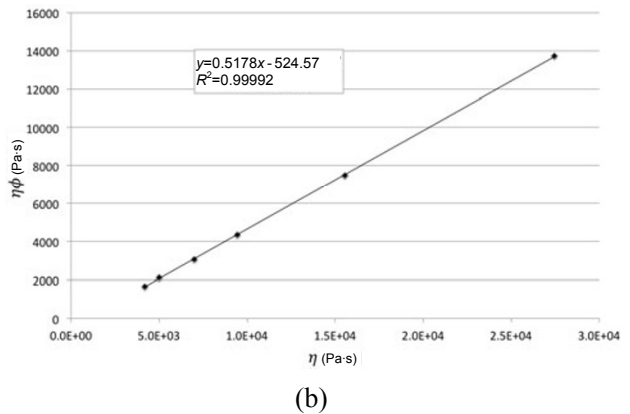
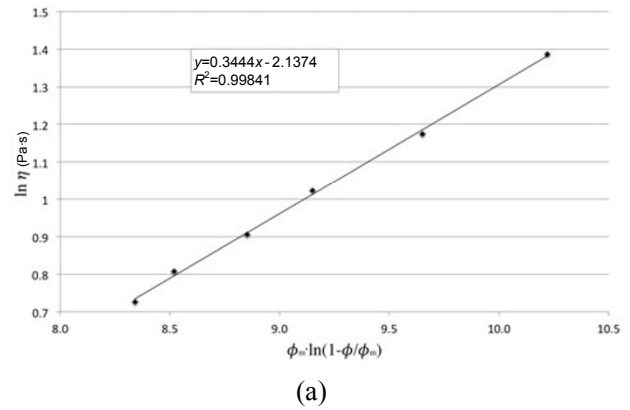


Fig. 11 Linearization and fit of (a) Krieger–Dougherty and (b) Reddy models. Fitting line equations and correlations factors are reported.

Table 2 Fitting parameters estimated from Fig. 11 for the two analyzed models

	$[\eta]$	η_0 (Pa·s)	ϕ_m
Krieger–Dougherty	2.90	498.4	0.54
Reddy	—	1013.1	0.52

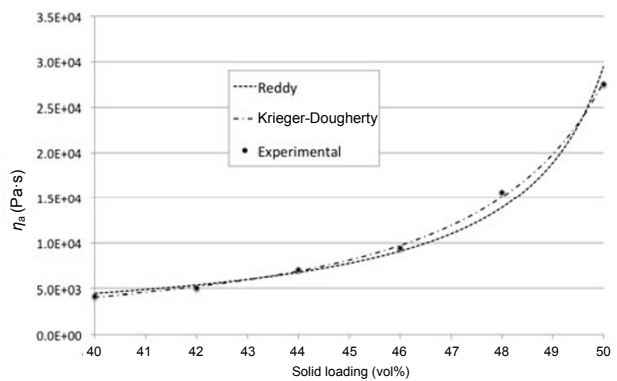


Fig. 12 Experimental apparent viscosity and trends calculated on the basis of Eqs. (3) and (4) with the parameters reported in Table 2.

obtained here, although the Krieger–Dougherty model seems to predict the relationship between η_a and ϕ slightly better in the analyzed range. The ϕ_m values obtained from the two different fits are substantially similar to that calculated from the linear extrapolation of the drying shrinkage to zero previously reported (0.542) (Fig. 5), thus confirming the goodness of the approach proposed in the present work.

4 Conclusions

In the formulation of a ceramic extrusion paste, the identification of the optimal range of solid loading has a great importance. Larger amount of powder causes high friction and liquid phase migration, while lower solid loadings correspond to very soft pastes unable to maintain the extruded shape. The upper limit of the range is typically defined as the maximum solid loading and corresponds to the optimal percentage of powder to be used in the extrusion of ceramic pastes. In the present work, the maximum solid loading in gadolinia-doped ceria pastes was determined by the extrapolation down to zero of the drying shrinkage of green extrudates formulated with variable solid loadings. The obtained value was compared to the analogous results determined by using two semi-empirical equations (Krieger–Dougherty and Reddy equations) describing the viscosity of high concentrated ceramic suspension as a function of the solid loading. The die wall shear stress, necessary for the evaluation of the viscosity, was also acquired, without need of any correction, by a novel method based on the analysis of the slope of the first stage of extrusion plot, corresponding to the flow of the paste through the die. The viscosities obtained by this approach were comparable to literature data reported for ceramic pastes with similar solid loading.

Acknowledgements

A. Azzolini would like to thank INSTM (Consorzio Interuniversitario Nazionale per la Scienza e Tecnologia dei Materiali) for co-funding this project as part of his Ph.D. research.

Open Access: This article is distributed under the terms of the Creative Commons Attribution License which permits any use, distribution, and reproduction

in any medium, provided the original author(s) and the source are credited.

References

- [1] Senapati PK, Panda D, Parida A. Predicting viscosity of limestone–water slurry. *Journal of Minerals and Materials Characterization and Engineering* 2009, **8**: 203–221.
- [2] Händle F. *Extrusion in Ceramics*. Springer, 2007.
- [3] Sigmund WM, Bell NS, Bergström L. Novel powder-processing methods for advanced ceramics. *J Am Ceram Soc* 2000, **83**: 1557–1574.
- [4] Vongheur H-O. Fundamentals of extrusion. *Manufacturing Confectioner* 2008, **88**: 71.
- [5] Chen ZC, Ikeda K, Murakami T, *et al.* Effect of particle packing on extrusion behavior of pastes. *J Mater Sci* 2000, **35**: 5301–5307.
- [6] August CR, Haber RA. Benbow analysis of extruded alumina pastes. *Whitewares and Materials: Ceramic Engineering and Science Proceedings* 2004, **25**: 15–22.
- [7] Kaya C, Blackburn S. Extrusion of ceramic tubes with complex structures of non-uniform curvatures made from nano-powders. *J Eur Ceram Soc* 2004, **24**: 3663–3670.
- [8] Benbow JJ, Jazayeri SH, Bridgwater J. The flow of pastes through dies of complicated geometry. *Powder Technol* 1991, **65**: 393–401.
- [9] Khan AU, Briscoe BJ, Luckham PF. Evaluation of slip in capillary extrusion of ceramic pastes. *J Eur Ceram Soc* 2001, **21**: 483–491.
- [10] Pabst W. Fundamental considerations on suspension rheology. *Ceram-Silikaty* 2004, **48**: 6–13.
- [11] Reddy JJ, Vijayakumar M, Mohan TRR, *et al.* Loading of solids in a liquid medium: Determination of CBVC by torque rheometry. *J Eur Ceram Soc* 1996, **16**: 567–574.
- [12] Liu F-J, Chou K-S. Determining critical ceramic powder volume concentration from viscosity measurements. *Ceram Int* 2000, **26**: 159–164.
- [13] Reddy JJ. Novel method for assessment of critical powder packing during powder forming. *Powder Metall* 1996, **39**: 281–285.
- [14] Wright JK, Edirisinghe MJ, Zhang JG, *et al.* Particle packing in ceramic injection molding. *J Am Ceram Soc* 1990, **73**: 2653–2658.
- [15] Liu D-M, Tseng WJ. Influence of solids loading on the green microstructure and sintering behaviour of ceramic injection mouldings. *J Mater Sci* 1997, **32**: 6475–6481.
- [16] Benbow JJ, Oxley EW, Bridgwater J. The extrusion mechanics of pastes—The influence of paste

- formulation on extrusion parameters. *Chem Eng Sci* 1987, **42**: 2151–2162.
- [17] Maca K, Pouchly V, Boccaccini AR. Sintering densification curve—A practical approach for its construction from dilatometric shrinkage data. *Sci Sinter* 2008, **40**: 117–122.
- [18] Perrot A, Lanos C, Estellé P, *et al.* Ram extrusion force for a frictional plastic material: Model prediction and application to cement paste. *Rheol Acta* 2006, **45**: 457–467.
- [19] Liu HJ, Liu J, Leu MC, *et al.* Factors influencing paste extrusion pressure and liquid content of extrudate in freeze-form extrusion fabrication. *Int J Adv Manuf Technol* 2012, **67**: 899–906.
- [20] Shaw HM, Edirisinghe MJ. Shrinkage and particle packing during removal of organic vehicle from ceramic injection mouldings. *J Eur Ceram Soc* 1995, **15**: 109–116.
- [21] Scherer GW. Theory of drying. *J Am Ceram Soc* 1990, **73**: 3–14.
- [22] Chotard T, Quet A, Ersen A, *et al.* Application of the acoustic emission technique to characterise liquid transfer in a porous ceramic during drying. *J Eur Ceram Soc* 2006, **26**: 1075–1084.
- [23] Rahaman MN, De Jonghe LC, Chu M-Y. Effect of green density on densification and creep during sintering. *J Am Ceram Soc* 1991, **74**: 514–519.
- [24] Özkan N, Briscoe BJ. Overall shape of sintered alumina compacts. *Ceram Int* 1997, **23**: 521–536.
- [25] Mukherjee A, Maiti B, Das Sharma A, *et al.* Correlation between slurry rheology, green density and sintered density of tape cast yttria stabilised zirconia. *Ceram Int* 2001, **27**: 731–739.
- [26] Bergström L. Colloidal processing of ceramics. In *Handbook of Applied Surface and Colloidal Chemistry*. Holmberg K, Ed. John Wiley & Sons, 2001: 201–218.
- [27] Reddy JJ, Ravi N, Vijayakumar M. A simple model for viscosity of powder injection moulding mixes with binder content above powder critical binder volume concentration. *J Eur Ceram Soc* 2000, **20**: 2183–2190.
- [28] Son Y. Determination of shear viscosity and shear rate from pressure drop and flow rate relationship in a rectangular channel. *Polymer* 2007, **48**: 632–637.
- [29] ASTM International. D3835-02 Standard test method for determination of properties of polymeric materials by means of a capillary rheometer. 2002.
- [30] Alfani R, Grizzuti N, Guerrini, GL, *et al.* The use of the capillary rheometer for the rheological evaluation of extrudable cement-based materials. *Rheol Acta* 2007, **46**: 703–709.
- [31] Yilmaz Z, Dogan M, Alkan M. Rheological and wall slip properties of kaolinite-silicon oil pastes during extrusion. *J Ceram Process Res* 2010, **11**: 752–759.